VORTEX FORMATION AND SHEDDING FROM A TWO-DIMENSIONAL, THIN, FLAT PLATE PARALLEL TO THE FREE STREAM

Thesis by

Andrew Burkhard Bauer

In Partial Fulfillment of the Requirements

For the Degree of

Aeronautical Engineer

California Institute of Technology

Pasadena, California

1959

ACKNOWLEDGEMENTS

I am very deeply grateful to the Douglas Aircraft Company, the California Institute of Technology, and GALCIT for making this research possible. The advice of Dr. Anatol Roshko has been helpful and inspiring, especially since recent developments in gas dynamics have tended to overshadow subjects relating to this thesis. Mrs. Virginia Sloan and Mrs. Walter Sheek typed the manuscript, and my wife Mary Ann provided the necessary encouragement for this study.

ABSTRACT

Vortex formation and shedding from the trailing edge of a two-dimensional, thin, flat plate parallel to the free stream is studied experimentally for the case of incompressible flow. Consideration of the classical boundary layer theory, the Karman vortex-street theory, the formation of the vortex centers, and some annihilation of vorticity in the free shear layers leads to an estimate of Strouhal number. This estimate is in reasonable agreement with experiment. The flow phenomena of a splitter plate mounted aft of the main plate and of a NACA 0012 airfoil are also observed experimentally and are found to be in essential agreement with applicable portions of the theory.

TABLE OF CONTENTS

PART	TITLE	PAGE
I	INTRODUCTION	1
II	EXPERIMENTAL APPARATUS	3
	Wind Tunnel	3
	Models	3
	Velocity Measurements	4
	Electronic Equipment	4
III	EXPERIMENTAL RESULTS	6
	Vortex Shedding Parameter F	6
	Flat Plate A	7
	Flat Plate B	7
	Flat Plate A with the Splitter Plate	9
	Boundary Layer and Vortex Measurements	9
	NACA 0012 Airfoil	10
IV	A THEORETICAL ESTIMATE OF THE VORTEX SHEDDING PARAMETERS	12
	The Karman Vortex-Street	12
	The Karman Momentum Relation	15
	Vortex Center Location	16
	Completion of the Physical Model	17
V	COMPARISON OF EXPERIMENTAL AND ESTIMATED RESULTS	18
	Flat Plates A and B	18
	Shedding Frequency Behavior at Large Values of δ^*/d	21

TABLE OF CONTENTS (CONT.)

PART	TITLE	PAGE
	Flat Plate A with the Splitter Plate	21
	NACA 0012 Airfoil	23
VI	CONCLUSIONS	24
	REFERENCES	26
	TABLES	27
	FIGURES	32

I. INTRODUCTION

The problem of the vortex shedding and flow field around bluff bodies is one of the oldest in fluid mechanics, but it remains one of the most important problems, both for practical and theoretical interest.

Two important contributions towards an understanding of this problem were made by the well-known studies of Kirchoff and Karman. Later, Roshko (1, 2, 3) used a form of the Kirchoff free-streamline theory "joined" to the Karman vortex-street theory to find a solution depending upon only one experimentally determined parameter. By allowing for some annihilation of the vorticity in the "free shear" layers near the separation point on the bluff body, this solution furnishes a useful correlation between different bluff cylinders as well as a further understanding of the flow mechanism.

The above contributions have been concerned primarily with cylindrical bodies having a length parallel to the flow equal to or less than the depth perpendicular to the flow.* However, many thin bodies, such as the thinner airfoil shapes, have flow fields of essentially the same nature. For this reason, this paper was initiated to study the flow at the base of thin, flat plates parallel

*Roshko (3) has also studied the considerable effects of a "splitter plate" placed behind the body.

to the free stream direction. These plates have rounded leading edges and bluff trailing edges.

It is readily apparent that the boundary layer thickness, being of the same order of magnitude or greater than the thickness of a "thin" plate, may have an important effect on the flow field and vortex shedding of the plate. Such has been found to be the case. In this respect, the problem for the thin plate differs from previous studies, where the boundary layer thickness has been sufficiently small to be of second order importance.

For thin, flat plates the usual flat plate boundary layer theory is applied, and it is assumed that the boundary layer thickness and the plate thickness play an essential role in determining the vortex-street formation. From this, a solution for the flat plate shedding frequency, represented by the usual Strouhal number S, is developed. This solution specifies the Karman vortex-street parameters and is found to agree within a few percent of the experimental results.

II. EXPERIMENTAL APPARATUS

Since the experiment required that vortex shedding be studied, hot wire and electronic equipment was found useful for measuring the frequency of the vortex velocity perturbations. The only other measuring devices on or near the models were several pressure orifices and a pitot-static tube.

No corrections were made to any of the measurements for tunnel wall effect. This was justified by the small thickness of the models with respect to the tunnel test section height. (Height to thickness ratio ranged from 18 to 500.)

Wind Tunnel. The experiments were all made in the GALCIT 20 - by 20 - inch low-turbulence tunnel. Wind velocity ranged from about 80 centimeters per second (2 miles per hour) to 2100 centimeters per second (47 miles per hour).

Models. Three two-dimensional models were tested (Fig. 1). The first two models were thin, flat plates with round leading edges and blunt trailing edges. The third model was an NACA 0012 section of 22.9 centimeters chord length. The flat plate A had a "splitter plate" which was mounted at varying distances downstream from the main plate. This splitter plate was used to effect changes in the vortex formation mechanism of the flow. Flat plate A also had two

pressure orifices, one in the middle of the base area and the other immediately ahead of the trailing edge.

Velocity Measurements. Free stream velocity was determined from the shedding frequency parameter F of a reference cylinder (0.635 centimeter in diameter), as described in (1). This reference shows that Reynolds number and free stream velocity are a unique function of F, and that F may be determined directly from the shedding frequency and the fluid viscosity. Velocities were also measured with a pitot tube. The pitot tube and other pressures were determined from a precision manometer to an accuracy of about .003 centimeter of alcohol. This measurement was compared to the shedding frequency parameters to obtain an extension to the curves of (1). Thus, once these curves were established, velocity could be determined by two different methods; however, accuracy of the pitot tube was poor for a speed less than about 400 centimeters per second.

Electronic Equipment. Hot wire equipment was used to read the frequency of vortex shedding and the wave form of the velocity fluctuations. The hot wire was a 0.12 mil tungsten wire mounted normal to the two-dimensional flow plane. Voltage fluctuations across the wire were amplified with a two-stage laboratory amplifier and were then fed into an oscilloscope. A Hewlett-Packard Model 202 B frequency

generator was calibrated against the 60 cycle line-voltage standard, and was used with the hot wire signal to produce Lissajous figures on the oscilloscope. The hot wire was mounted on a traversing mechanism accurate to about 0.005 centimeter, traversing normal to the free stream direction.

III. EXPERIMENTAL RESULTS

A Karman vortex-street appeared in the wakes of all models and at all Reynolds numbers tested. It appeared on the oscilloscope as a double row of periodic velocity fluctuations of alternate spacing. The alternate spacing was apparent from the waveform and the double frequency read near the wake center line.

Vortex Shedding Parameter F. In (1) the parameter $F \equiv \frac{n d^2}{\nu}$ was shown to be a function of R_o and was experimentally determined for a circular cylinder. Here n = shedding frequency, d = cylinder diameter, ν = kinematic viscosity, and R_o = Reynolds number based on d. For the present report, this relation has been extended by piecewise curve fitting up to $R_o = 9500$ as:

$$F = .205\ R_o + 12 \qquad 2000 < R_o < 5500$$

$$F = .190\ R_o + 95 \qquad 5500 < R_o < 9500$$

based on the test points shown in Fig. 2. The similar relations of (1) are:

$$F = .212\ R_o - 4.5 \qquad 50 < R_o < 150$$

$$F = .212\ R_o - 2.7 \qquad 300 < R_o < 2000$$

These four relations were used to compute R_o and the free stream velocity for the remainder of the experimental results (F is known from experimental values of n and ν), as low speed velocity measurements could be obtained more accurately by this means than by the direct measurements of the pitot-static tube.

Flat Plate A. This plate was tested for shedding frequency and base pressures over a Reynolds number* range of 17,600 to 460,000, as shown in Figs. 3, 4, and 5, and in Table 1. At the high end of the range the boundary layer and the vortex shedding became turbulent in character and the shedding frequency became rather difficult to read. At all speeds the Karman vortex-street was detected aft of the model, as expected. Over the model and in the model boundary layer, no significant velocity perturbations other than those of the turbulent boundary layer were observed; however, as the hot wire probe was moved aft past the trailing edge, vortex shedding appeared. Actually, this shedding first became measurable at about one plate thickness length ahead of the trailing edge, and developed to essentially full amplitude at a distance of the order of four plate thicknesses aft of the trailing edge.

Surface pressure measurements were taken at the base center line and also immediately ahead of the trailing edge, as shown on Fig. 5 and Table 1.

Flat Plate B. Plate B was tested over a Reynolds number range of 16,400 to 270,000, as shown in Figs. 3 and 6 and in Table 2. At a Reynolds number of about 270,000 the vortex shedding pattern on the oscilloscope would alternate

* Reynolds number R for all the models is based on the model chord length ℓ.

between laminar and turbulent appearance. More precisely, the "laminar" pattern appeared as a smooth function, approximating a sine wave on the oscilloscope. Several times a second the "turbulent" pattern appeared as a function with many sharp peaks, etc. Somewhat higher Reynolds numbers were also tested, but the pattern was completely turbulent, and no single dominant shedding frequency could be found. At the same time, turbulence was also noted in the boundary layer.

At Reynolds numbers less than about 40,000, there also appeared to be some slight velocity fluctuation in the boundary layer of the same frequency as the Karman vortex-street. At the same time, a second, lower frequency of about 30 cycles per second appeared to modulate the Karman vortex-street. As Reynolds number was decreased, the amplitude of the second frequency became greater with respect to the original frequency. At a Reynolds number of 34,000 the two frequencies appeared to be of equal amplitude. This trend continued until only the second frequency was observed at a Reynolds number of 26,000. A third frequency of about 19.5 cycles per second appeared at still lower Reynolds numbers and became equal to the second at a Reynolds number of about 20,500. This trend continued to the end of the tests at a Reynolds number of 16,400. The fact that only the dominant frequency could be accurately measured accounts for the "jumps" in Figs. 3 and 6.

Flat Plate A with the Splitter Plate. Fig. 7 and Table 3 show the effect of a "splitter plate" (see Fig. 1) located aft of the model. With the splitter plate close to the trailing edge, the splitter plate appeared to form a new vortex shedding pattern of lower frequency than that of the single plate. For all positions of the splitter plate, the vortex shedding fluctuations started near the main trailing edge, but modified in frequency by the splitter plate. Also, smaller amplitude oscillations of higher frequency were sometimes present, but their frequency could not be measured. Of course, the far aft positions of the splitter plate produced a flow pattern similar to that for no splitter plate at all. It is interesting to note that S and pressure coefficient C_p jump in the manner shown for the splitter plate behind the circular cylinder of Fig.4,(3).

Surface pressure measurements were taken at the base center line and immediately ahead of the trailing edge.

Boundary Layer and Vortex Measurements. As a check of the flow pattern of Plate B, a pitot tube was moved through the boundary layer in order to measure the velocity profile. This velocity profile, taken at approximately 1.5 plate thickness ahead of the trailing edge, is shown in Fig. 8. It shows good agreement with the Blasius theory. A profile was also taken at 0.5 plate thickness downstream of the trailing edge. This gave similar results, but showed

higher velocities close to and on the plane of the plate surface. The trailing edge boundary layer thickness was approximately 0.8 plate thickness during this test.

Fig. 8 also shows the result of using a voltmeter to measure relative amplitudes of the velocity fluctuations across the vortex street. Here the probe was located approximately 5 plate thicknesses downstream from the model. This shows a pattern like that qualitatively observed for all the vortex street measurements.

NACA 0012 Airfoil. This airfoil was tested at Reynolds numbers from approximately 15,000 to 90,000 (see Fig. 3 and Table 4). Tests were stopped at the high end of the range as the shedding frequency became somewhat variable or turbulent as Reynolds number increased, until it no longer could be read. At all Reynolds numbers tested, the vortex street appeared in the wake, as with the flat plate models. It is interesting that no significant velocity fluctuations or vortices appeared until immediately downstream of the trailing edge.

At Reynolds numbers in the neighborhood of 60,000 a jump in shedding frequency appeared, and there was a small range over which both frequencies were possible, but only one at a time. As a matter of fact, at one test point (R = 62,800) the oscilloscope showed a rather random jumping between the two frequencies without any observable

change in the tunnel or model operating conditions. The shedding frequency would stay at one, well-defined value for a period of the order of 5 to 30 seconds and then suddenly jump to the other, also well-defined value. This jumping from one value to the other was observed to continue for several minutes until the tunnel speed was changed. It was assumed that this jumping might be the result of the transition point changing between two locations.

IV. A THEORETICAL ESTIMATE OF THE VORTEX SHEDDING PARAMETERS

In order to better understand the experimental results, a physical model is here developed to estimate the shedding parameters for the thin, flat plate body. This model is based on the Karman vortex-street and on boundary layer theory. Incompressible flow is assumed throughout the derivation.

The Karman Vortex-Street. It is assumed that the vortex street behind a thin, flat plate is approximated by the classical Karman vortex-street theory. In actuality, it is known (1) that the fluid viscosity results in a viscous core formation in place of the potential vortex centers; also, the vortex street is dissipated far downstream of the plate. However, these effects are assumed to be of second order importance for the present discussion.

The Karman vortex-street theory (4 and 5) states that the vortices move at a speed

$$V = \frac{\Gamma}{2\sqrt{2}\,a} \qquad (1)$$

with respect to the free stream, where Γ is the circulation of a single vortex, and a is the streamwise distance between vortices. Hence, the circulation per unit time developed in each half of the vortex street behind a bluff body is $\Gamma\left(\frac{U-V}{a}\right)$, where U is the free-stream velocity.

Now, over a sufficiently thin, flat plate, the velocity outside the boundary layer is the free-stream velocity U. The velocity at the edge of the boundary layer is related directly to the circulation in the boundary layer. That is, the rate at which circulation flows past any plane section normal to a boundary layer is:

$$\int_0^{\delta} f\, u\, d\eta = \frac{U^2}{2}$$

where f is the local vorticity, u is the local velocity in the boundary layer, η is the coordinate normal to the plate, and δ is the boundary layer thickness. If we let ϵ be the fraction of the boundary layer vorticity that is not lost by viscous diffusion between the plate trailing edge and the formation of the vortex street, that is, the fraction which forms the vortex street, we can equate:

$$\frac{\epsilon U^2}{2} = \Gamma\left(\frac{U - V}{a}\right) \tag{2}$$

Solving (1) and (2) for $\frac{\Gamma}{a}$, we get:

$$\frac{\Gamma}{a} = \sqrt{2}\, U\left[1 - \sqrt{1 - \frac{\epsilon}{\sqrt{2}}}\right] \tag{3}$$

and

$$V = \frac{U}{2}\left[1 - \sqrt{1 - \frac{\epsilon}{\sqrt{2}}}\right] \tag{4}$$

where the sign of the radical is determined as follows: Since the average velocity in the median plane of the vortex is $\frac{\Gamma}{a}$ with respect to the free stream (5), this velocity is greater than U for the radical sign assumed positive.

This appears to be physically unrealistic; also, it is not compatible with the experimental results. Hence, the sign has been taken as negative.

The shedding frequency n, the number of vortices formed per unit time in <u>each</u> side of the vortex street, must then be given by:

$$n = \frac{U-V}{a} = \frac{U}{2a}\left[1 + \sqrt{1 - \frac{\epsilon}{\sqrt{2}}}\right] \qquad (5)$$

Since the spacing b between vortex rows in the street is given by b = .281 a, we have:

$$n = \frac{U}{b\,\eta_1(\epsilon)} \qquad (6)$$

where

$$\eta_1(\epsilon) = \frac{2}{.281\left[1 + \sqrt{1 - \frac{\epsilon}{\sqrt{2}}}\right]} \qquad (7)$$

Values of $\eta_1(\epsilon)$ are shown in Fig. 9.

The dimensionless shedding frequency, Strouhal number, is defined by: $S \equiv \frac{n\,d}{U}$

and hence

$$S = \frac{d}{b\,\eta_1(\epsilon)} \qquad (8)$$

where d is a characteristic length of the body. For this report, d is taken as the thickness of the plate.

Since these relations are based on only the boundary layer vorticity and the Karman vortex-street, it is clear that they should form a basis for the rest of the theory.

The Karman Momentum Relation. Von Karman has derived, from considerations of momentum (4 and 5), the formula

$$C_D = \frac{b}{d}\left[5.65\left(\frac{V}{U}\right) - 2.25\left(\frac{V}{U}\right)^2\right]$$

where C_D is the body drag coefficient based on d. Using equation (4), which gives $\frac{V}{U} = \frac{V}{U}(\epsilon)$, we may write

$$C_D = \frac{b}{d}\,\eta_2(\epsilon) \tag{9}$$

$\eta_2(\epsilon)$ is plotted on Fig. 9. Hence, the Karman value of C_D depends on only the street width ratio $\frac{b}{d}$ and the value of ϵ.

C_D for the thin plate also may be computed as the sum of the base pressure drag and the skin friction or boundary layer momentum thicknesses, which gives:

$$C_D = -C_P + \frac{4\theta}{d} \tag{10}$$

where θ is the boundary layer momentum thickness of one side of the plate.

By eliminating C_D from (9) and (10), we get the base pressure coefficient:

$$C_P = \frac{4\theta - b\,\eta_2(\epsilon)}{d} \tag{11}$$

Thus, C_p is related directly to the boundary layer momentum thickness and the Karman vortex-street parameters $\frac{b}{d}$ and ϵ.

Vortex Center Location. The vortex centers of the street begin forming in the "free shear" layers, which start at the plate trailing edge. This concept is used to write the relation

$$b = d + 2\delta^* + \lambda C_p d \qquad (12)$$

where δ^* is the boundary layer displacement thickness in the neighborhood of the plate trailing edge, and λ is a dimensionless empirical parameter. The sign of λ is assumed positive.

This relation is based on the assumption that the vortices first form at distance δ^* away from each side of the plate, giving a street width of $d + 2\delta^*$. As the vortex centers move downstream from the plate, the base pressure is assumed to change the width by amount $\lambda C_p d$. The sign of this term is reasonable, inasmuch as a negative C_p, for example, might be expected to "pull in" the vortex centers, whereas a positive C_p would be expected to do the opposite. The magnitude of the parameter λ will be based on experimental results.

The distance δ^* is used above, inasmuch as it represents an effective thickness added to the plate, as seen by the potential flow outside the boundary layer. δ^* is also the weighted average distance between the plate and the boundary layer vorticity, as a little computation easily shows. Thus, two different points of view give the same location of vortex center formation.

Completion of the Physical Model. By using equations (11) and (12) to eliminate C_p, we get:

$$\frac{b}{d} = \frac{1 + \frac{\delta^*}{d}\left(2 + \frac{4\lambda\theta}{\delta^*}\right)}{1 + \lambda\eta_2} \tag{13}$$

Then, putting equation (13) into equation (4), S becomes:

$$S = \frac{1 + \lambda\eta_2}{\eta_1\left[1 + \frac{\delta^*}{d}\left(2 + \frac{4\lambda\theta}{\delta^*}\right)\right]} \tag{14}$$

Hence, the Karman vortex-street parameters depend only on the parameters $\frac{\delta^*}{d}$, ϵ, λ, and the boundary layer profile parameter $\frac{\theta}{\delta^*}$. Both ϵ and λ are based on experimental results, while $\frac{\delta^*}{d}$ and $\frac{\theta}{\delta^*}$ usually may be computed from boundary layer theory.

The parameter λ for the computations of this paper has been taken as unity, which gives a fair agreement to experimental results. However, varying λ between 0 and 1 gives only a small contribution to S and C_p for the values of $\frac{\delta^*}{d}$, ϵ, and $\frac{\theta}{\delta^*}$ used in this paper. In particular, if we assume $\epsilon = 0.5$, $\frac{\delta^*}{d} = 1.1$, and a laminar boundary layer profile, then equation (14) will give the same value of S for either $\lambda = 1.0$ or $\lambda = 0$.

V. COMPARISON OF EXPERIMENTAL AND ESTIMATED RESULTS

Flat Plates A and B. The experimental values of Strouhal number for plates A and B are plotted in terms of $\frac{\delta^*}{d}$ in Fig. 10. Values of Strouhal number estimated from equation (14) are also plotted. The boundary layer parameters δ^* and θ have been computed from the usual boundary layer equations for flat plates (see reference 6, for example), assuming that the plate thickness is sufficiently small to be neglected. Equations (13) and (11) were used in the same manner to compute C_p, as plotted on Fig. 5.

The experimental results at Reynolds numbers greater than about 300,000 indicated that the boundary layer flow was becoming turbulent. This appeared both from the waveform observations and from the Strouhal number behavior shown in Fig. 4. Hence, the boundary layer parameters used in equations (11), (13) and (14) were the usual laminar profile relations for Reynolds number less than 300,000. However, since the theory of turbulent flow is not well formulated near the transition region, no simple boundary layer parameters were available for the assumed turbulent flow region. This was particularly true since the transition point (or region) itself is not well defined. For these reasons, the boundary layer relations used for Reynolds numbers greater than 300,000 of Figs. 5

and 10 were the well-known fully turbulent flow parameters (based on the one-seventh power velocity profile computed from the leading edge). Therefore, where turbulent flow is indicated on Figs. 5 and 10, the estimated parameters are not expected to be as close to experiment as for the case of laminar flow.

It should be remarked that the low turbulence level of the flow of the GALCIT 20-inch wind tunnel might be expected to delay transition to a Reynolds number considerably greater than 300,000. However, since the unsteady vortex street was located close to the end of the boundary layer flow, it appears that a transition Reynolds number in the neighborhood of 300,000 is a reasonable number. Such a transition Reynolds number has been reported by many observers for cases where the free stream turbulence level is not too low (see reference 6).

The experimental results are seen to be in fair agreement with the estimate for $\lambda = 1$, $\epsilon = 0.5$, and a laminar boundary layer. This agrees well with the value $\epsilon = 0.5$ for circular cylinders reported in reference 3. Also, there appears to be a trend toward small ϵ as Reynolds number decreases and δ^* increases.

It is interesting that the Strouhal number estimated for the fully turbulent boundary layer is close to the "turbulent" experimental values. However, C_p and S indicate contradictory values of ϵ, and it is clear that

more knowledge of the boundary layer is needed to obtain any better agreement between experiment and estimated values of C_p and S.

It should be noted that some improvement between the experimental and the estimated valued of S and C_p may be obtained if λ is taken somewhat less than unity. For flat plate A, a decrease in λ will decrease the estimated values of both S and C_p. By this means the slight contradiction between values of ϵ of Figs. 5 and 10 may be reduced to within the range of experimental error.

A "wake Strouhal number", similar to that of reference 3, is defined as

$$S^* = \frac{n(d+2\delta^*)}{U_s}$$

where $U_s = \sqrt{1-C_p}\, U$.

Here $d+2\delta^*$ is representative of the estimated distance between vortex centers in the wake, and U_s represents the "free streamline" velocity assumed to exist in potential flow at the edge of the wake. Values of S* computed from experiment are presented on Fig. 11 for the case of flat plates A and B. (For plate B the value of C_p is assumed to be 0.) This data, when compared to Fig. 4, shows the leveling effect of using S*, but the values of S* are considerably greater than that for the several models tested in reference 3, where S* = 0.16 was obtained.

Shedding Frequency Behavior at Large Values of $\frac{\delta^*}{d}$. On flat plate B the parameter $\frac{\delta^*}{d}$ is larger than on flat plate A, and apparently is related to the odd experimental behavior at $\frac{\delta^*}{d}$ greater than about 2.7 (Reynolds numbers less than about 35,000). Here the total boundary layer thickness of both sides of the plate is greater than 16 times the plate thickness. Also, the flow has a Reynolds number based on $d+2\theta$ which is approaching the somewhat unstable "transition range" of reference 1. However, it is interesting to note that the estimated value of Strouhal number (for ϵ near 0.5) is found to pass through the region covered by the experimental points.

It is assumed that the above behavior may be a result of shear layer oscillations such as mentioned by Tani in reference 7. Tani has obtained experimental data for the oscillation frequency of flow past a square corner. However, the available literature and the experimental data are not sufficient to make any definite statements concerning this.

Flat Plate A with the Splitter Plate. As shown in Fig. 7, the splitter plate causes two jumps in Strouhal number as it moves toward the main plate. Using these values of S in equation (8), the basic vortex street relation, we see that the street width b is increased approximately six times, regardless of the value of ϵ used. It may be expected

that equations (11) through (14) hold; however, for the splitter plate located close to plate A, the vortex shedding must be controlled by the trailing edge of the splitter plate. The flow must separate from the trailing edge of plate A and reattach on the splitter plate. Thus, it is likely that a thick boundary layer is formed on the splitter plate. This increased thickness of the boundary layer flow then greatly increases the value of b.

It is also remarkable to note that a gap of only about three times the main plate thickness is sufficient to restore the flow pattern to essentially that for no splitter plate at all. This leads to the conclusion that once the vorticity has had a sufficient opportunity to "roll up" into concentrated street form, a splitter plate makes little difference.

NACA 0012 Airfoil. None of the above theory may be applied directly to the NACA 0012 airfoil data of Fig. 3 inasmuch as there is not a well-defined separation point. Also, near the separation point the potential flow velocity is expected to be greater than the free stream velocity, so that the vorticity shed may lead to a new form for the parameter $\eta_1(\epsilon)$. However, assuming $\eta_1 = 4.62$, equation (8) gives b = 1.38 centimeter for S = .43 (R = 23,000 or R = 64,000 in Fig. 3, where S is based on airfoil maximum thickness). Thus, it appears that b is only about one-half the maximum thickness of the airfoil. This appears reasonable in light of the theory and computations for flat plates.

It is assumed that the jump and the decreasing value of Strouhal number, as Reynolds number becomes greater than 60,000, are associated with boundary layer phenomena. Both the jump and the decrease in Strouhal number may be caused by a shift in the separation point to a point further downstream. This is different from the flat plate case, where separation is always assumed to occur at or very close to the trailing edge. Transition may also play a role in determining the separation point and the observed phenomena.

VI. CONCLUSIONS

An experimental investigation and theoretical estimate of the parameters of the Karman vortex-street shed behind an NACA 0012 airfoil and behind thin, flat plates in incompressible flow has indicated the following conclusions:

1. Consideration of the Karman vortex-street theory, the formation of the vortex centers, and boundary layer parameters leads to an estimate of Strouhal number S for flat plates. This estimate depends only on the ratio of boundary layer displacement thickness to plate thickness $\frac{\delta^*}{d}$, the boundary layer profile parameter $\frac{\theta}{\delta^*}$, an empirical parameter λ, and a vorticity annihilation parameter ϵ. For a value of $\epsilon = 0.5$ and a laminar boundary layer, this estimate is within a few percent of the experimental results. The estimate of pressure coefficient C_p on the base of the plate is also close to the experimental value for $\epsilon = 0.5$.

2. For values of $\frac{\delta^*}{d}$ greater than about 2.7, more than one shedding frequency appeared in the wake of the plate.

3. The introduction of a "splitter plate" immediately aft of the main plate inhibits the vortex street formation to much smaller values of S and ϵ. The street width b is greatly increased.

4. Vortex shedding from a NACA 0012 airfoil section appears similar to that for flat plates. However, since the boundary layer development and the separation point on the airfoil are not as well understood as with flat plates, no shedding frequency estimate has been made for the airfoil.

REFERENCES

1. Roshko, Anatol: "On the Development of Turbulent Wakes from Vortex Streets", NACA TR 1191, (1954).

2. Roshko, Anatol: "A New Hodograph for Free-Streamline Theory", NACA TN 3168, (1954).

3. Roshko, Anatol: "On the Drag and Shedding Frequency of Two-Dimensional Bluff Bodies", NACA TN 3169, (1954).

4. Von Karman, Th., and Rubach, H.: "Uber den Mechanismus des Flussigkeits und Luftwiderstandes", Phys. Zs., Bd.13, Heft 2, Jan. 15, 1912, pp. 49-59.

5. Lamb, Horace: "Hydrodynamics", Sixth ed., Dover Publications,(1945).

6. Schlichting, Hermann: "Boundary Layer Theory", Pergamon Press, (1955).

7. Tani, Itiro, and Sato, H.: "Boundary Layer Transition by Roughness Element", Journal of the Physical Society of Japan, vol. 11, p. 1284, (1956).

TABLE 1

EXPERIMENTAL DATA FOR FLAT PLATE A

U (cm./sec.)	R	$\tilde{n}$ (cycles/sec.)	S	C_p	C_{ps}*
83.4	17,600	14.2	.1082		
94.5	20,000	17.1	.1150		
109.2	23,100	19.6	.1138		
121.7	25,750	23.0	.1200		
131.7	27,800	26.3	.1267		
149	31,400	30.5	.1300		
161	34,000	34.5	.1360		
198	41,900	44.0	.1412		
251	53,000	61.0	.1545	-0.28	-0.17
303	64,100	77.5	.1625	-0.35	-0.15
356	75,400	97.0	.1732	-0.290	-0.158
418	88,400	119.5	.1814	-0.313	-0.176
485	102,500	146.0	.1912	-0.273	-0.137
573	121,200	177	.1965	-0.320	-0.180
688	145,500	222	.2050	-0.308	-0.140
825	174,500	277	.2133	-0.318	-0.153
990	209,500	340	.2180	-0.333	-0.162
1,124	237,600	389	.2195	-0.312	-0.162
1,336	282,000	449	.2133	-0.323	-0.147
1,569	330,500	463	.1875	-0.312	-0.143

*Note: C_{ps} = pressure coefficient on the model surface.

TABLE 1 (CONT.)

EXPERIMENTAL DATA FOR FLAT PLATE A

U (cm./sec.)	R	ν (cycles/sec.)	S	C_p	C_{ps}
1,815	383,000	534	.1868	-0.337	-0.155
2,050	432,000	600	.1860	-0.338	-0.145
2,180	460,000	642	.1870	-0.350	-0.152

TABLE 2

EXPERIMENTAL DATA FOR FLAT PLATE B

U (cm./sec.)	R	ν (cycles/sec.)	S
79.2	16,400	19.2	.0246
91.7	19,000	19.8	.0219
95.9	19,900	19.4	.0205
100.5	20,800	29.7	.0300
112.0	23,200	29.7	.0269
126.2	26,200	29.7	.0239
140.5	29,100	29.7	.0214
150.5	31,200	29.7	.0200
157.4	32,600	29.7	.0191
165.4	34,200	25.8	.0158
165.4	34,200	52.3	.0321

TABLE 2 (CONT.)

EXPERIMENTAL DATA FOR FLAT PLATE B

U (cm./sec.)	R	n (cycles/sec.)	S
171.2	35,400	52.3	.0310
180	37,300	54.2	.0306
217	45,100	72.2	.0338
253	53,500	90.2	.0362
307	63,600	124.1	.0411
366	75,900	156	.0433
426	88,300	209	.0498
485	100,300	256	.0536
573	118,500	338	.0599
689	142,500	444	.0654
836	173,000	583	.0707
1,012	209,500	740	.0742
1,112	230,000	851	.0777
1,212	250,500	985	.0825
1,302	269,500	1,025	.0798

TABLE 3

EXPERIMENTAL DATA FOR FLAT PLATE A

WITH THE SPLITTER PLATE

U = 485 cm./sec.

R = 99,800

Gap between plates (in thicknesses of Plate A)	n (cycles/sec.)	S	Cp	Cps
0.56	25.4	.0333	-.07	-.04
0.63	25.5	.0334	-.07	-.07
1.00	25.0	.0327	-.07	-.07
1.13	24.7	.0324		
1.25	81.7	.1070	-.10	-.07
1.50	81.0	.1060	-.08	-.07
1.75	80.5	.1054		
1.88	134.7	.1763		
1.96	139.5	.1827		
2.00	137.6	.1800	-.07	-.07
3.00	135.7	.1777	-.25	-.11
5.00	139.5	.1827	-.27	-.14
7.50	143.3	.1880	-.30	-.17
12.00	145.3	.1905	-.28	-.17
∞	145.3	.1905	-.28	-.14

TABLE 4

EXPERIMENTAL DATA FOR NACA 0012 AIRFOIL

U (cm./sec.)	R	n (cycles/sec.)	S
98.1	15,300	13.0	.364
105.3	16,400	14.3	.372
129.5	20,200	19.4	.411
161.0	25,150	26.5	.451
202.7	31,600	35.6	.481
256.2	40,100	48.4	.518
312.0	48,700	65.5	.576
354	55,100	77.6	.601
368	57,300	84.4	.629
372	58,000	84.4	.621
377	58,600	61.6	.449
382	59,500	86.3	.619
385	60,000	61.1	.435
396	61,600	62.5	.433
403	62,800	63.5	.432
403	62,800	91.2	.621
411	64,100	64.5	.430
456	71,100	72.3	.434
459	71,500	71.3	.426
501	78,100	77.1	.422
571	89,100	86.3	.414
679	105,800	95.0	.390

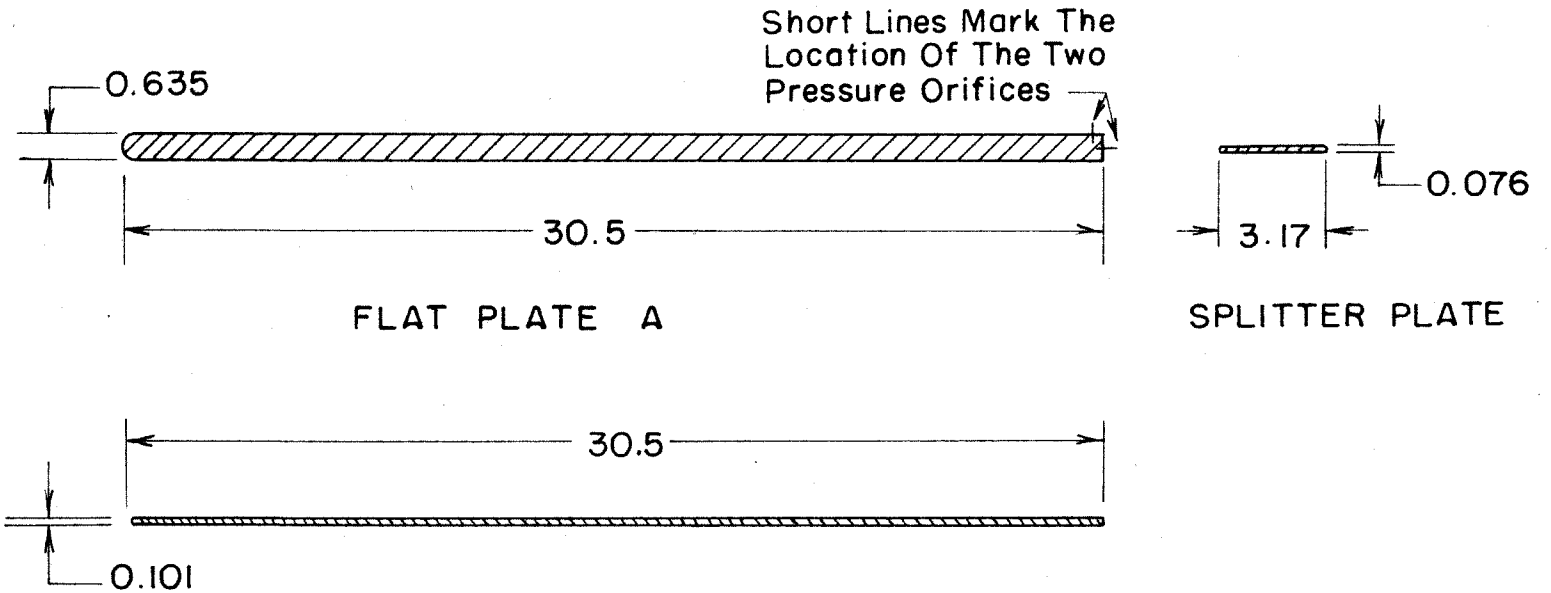

Note:
1. Plate Leading Edges Are Round
2. Dimensions Are In Centimeters

FIG. 1 – CROSS SECTIONS OF FLAT PLATE MODELS

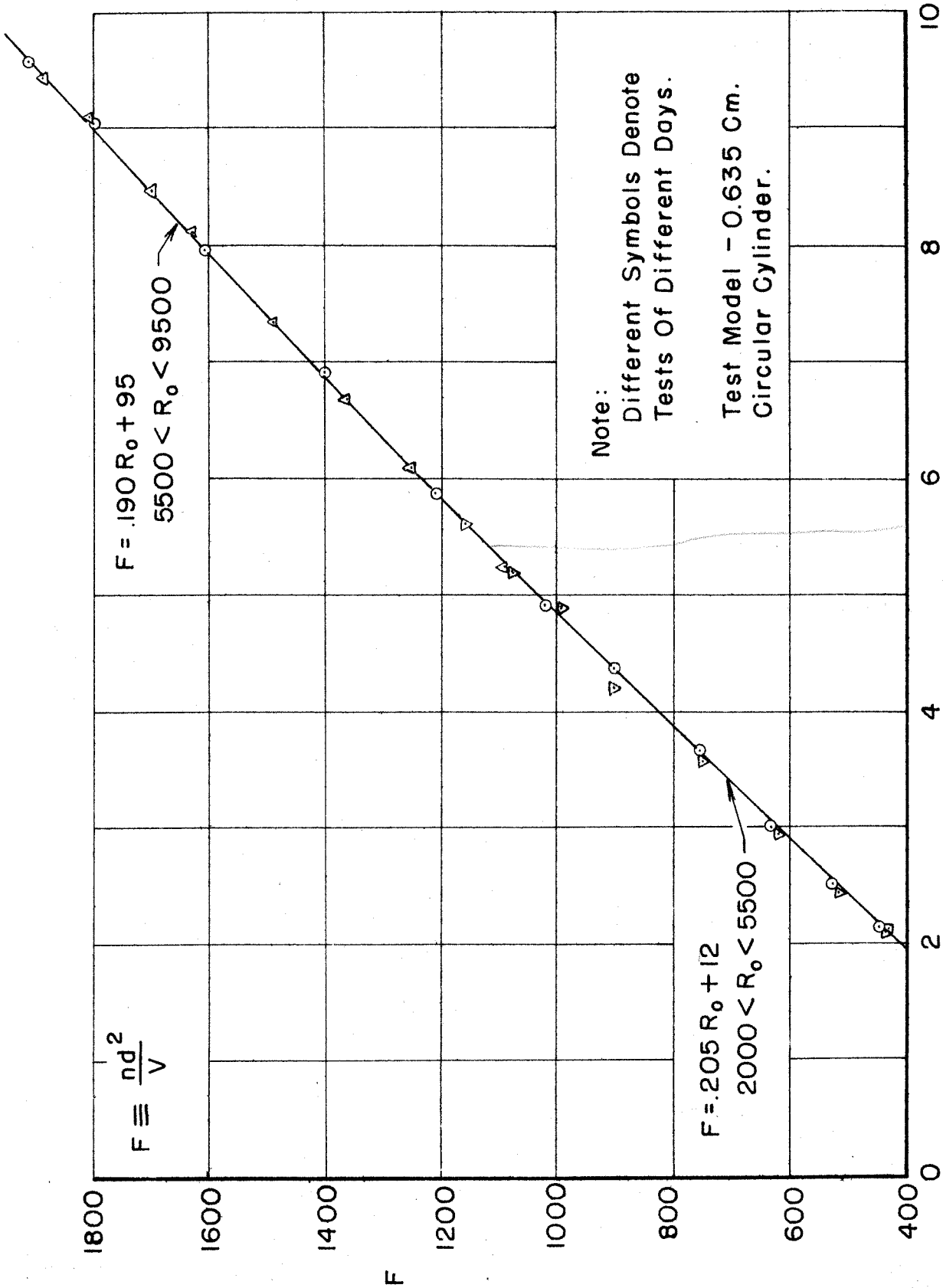

FIG. 2 - EXPERIMENTAL F VS. REYNOLDS NUMBER

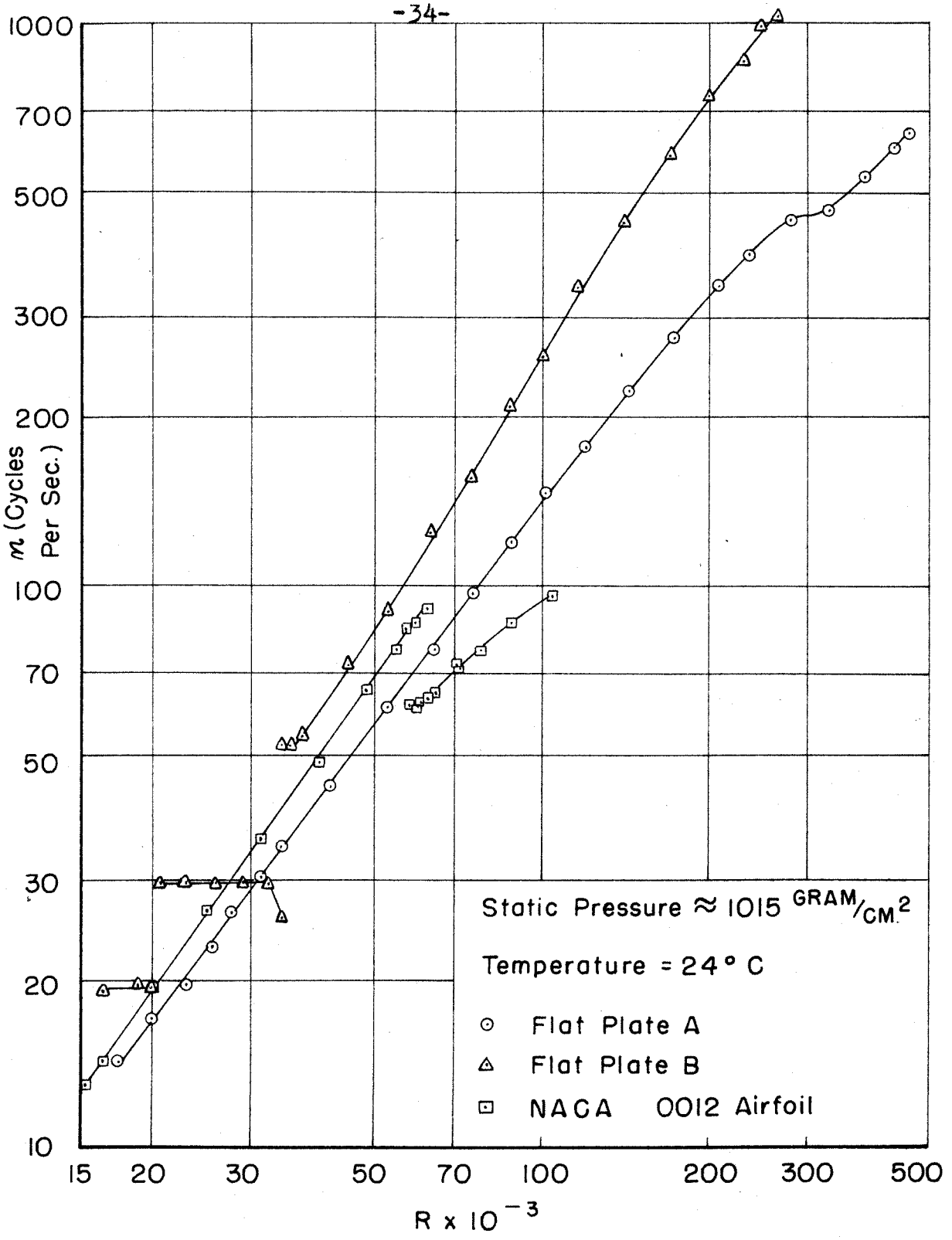

FIG. 3 – EXPERIMENTAL SHEDDING FREQUENCY VS. REYNOLDS NUMBER

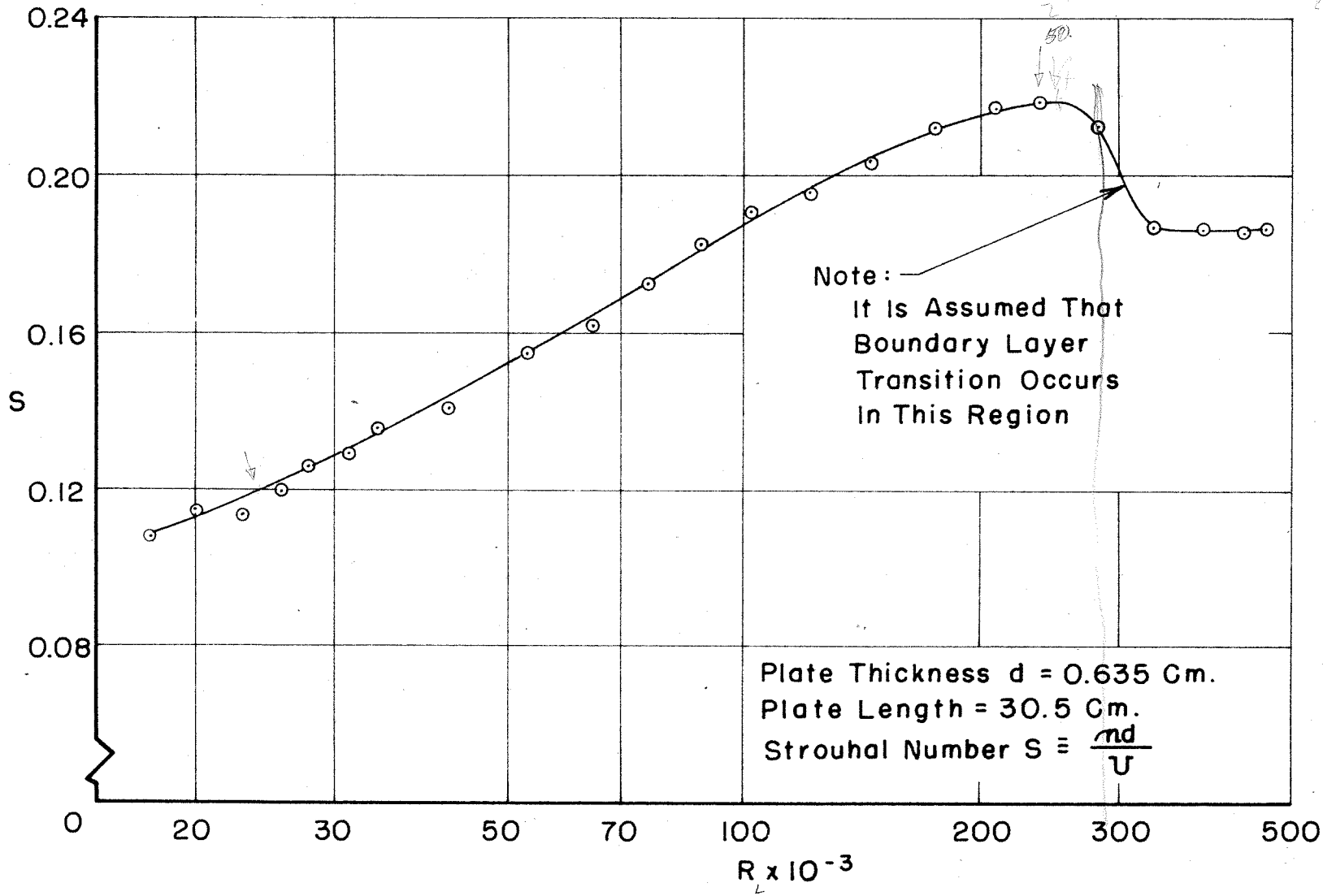

FIG. 4 – FLAT PLATE A – STROUHAL NUMBER VS. REYNOLDS NUMBER

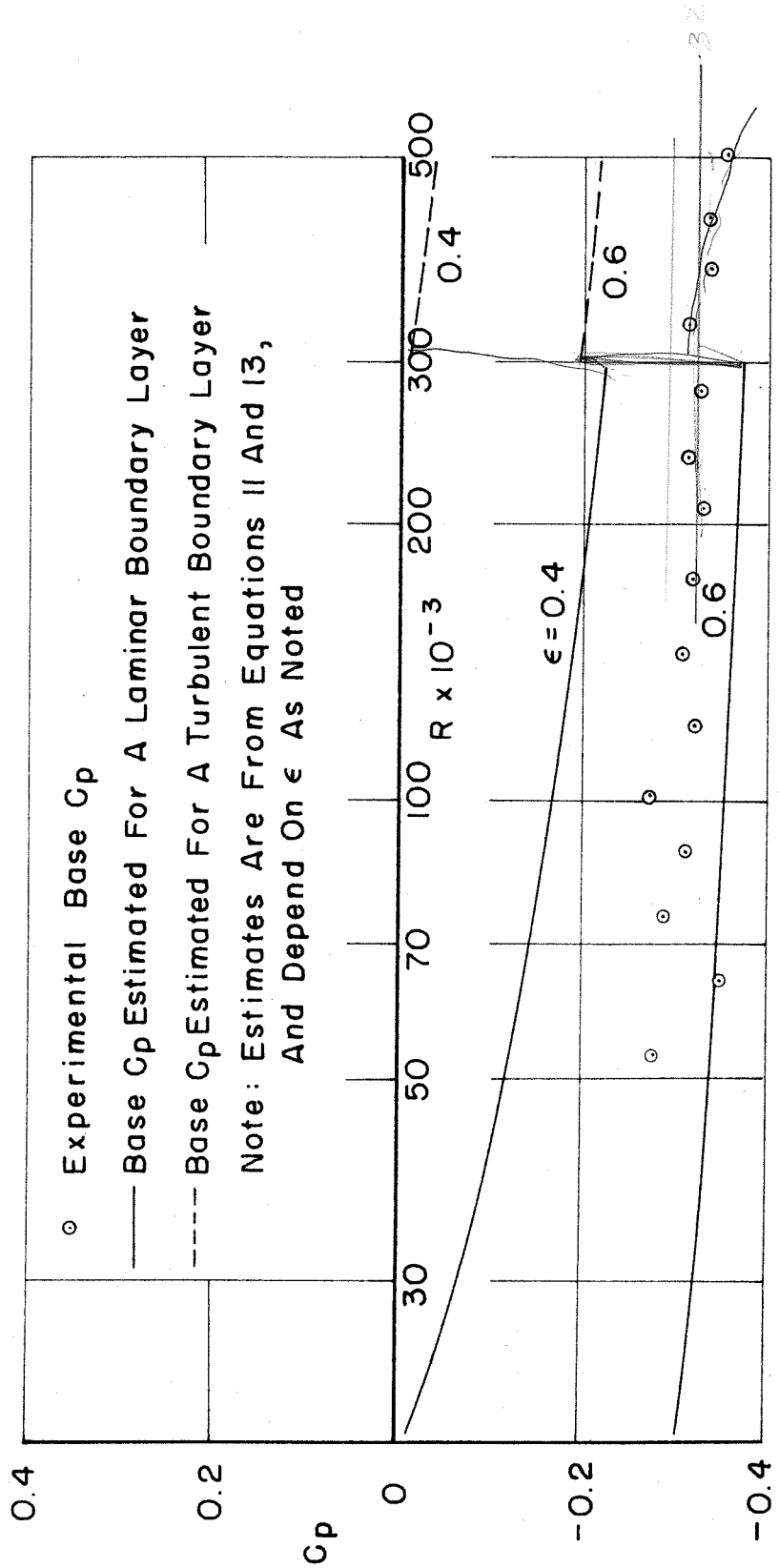

FIG. 5 - FLAT PLATE A - ESTIMATED AND MEASURED VALUES OF BASE PRESSURE COEFFICIENT

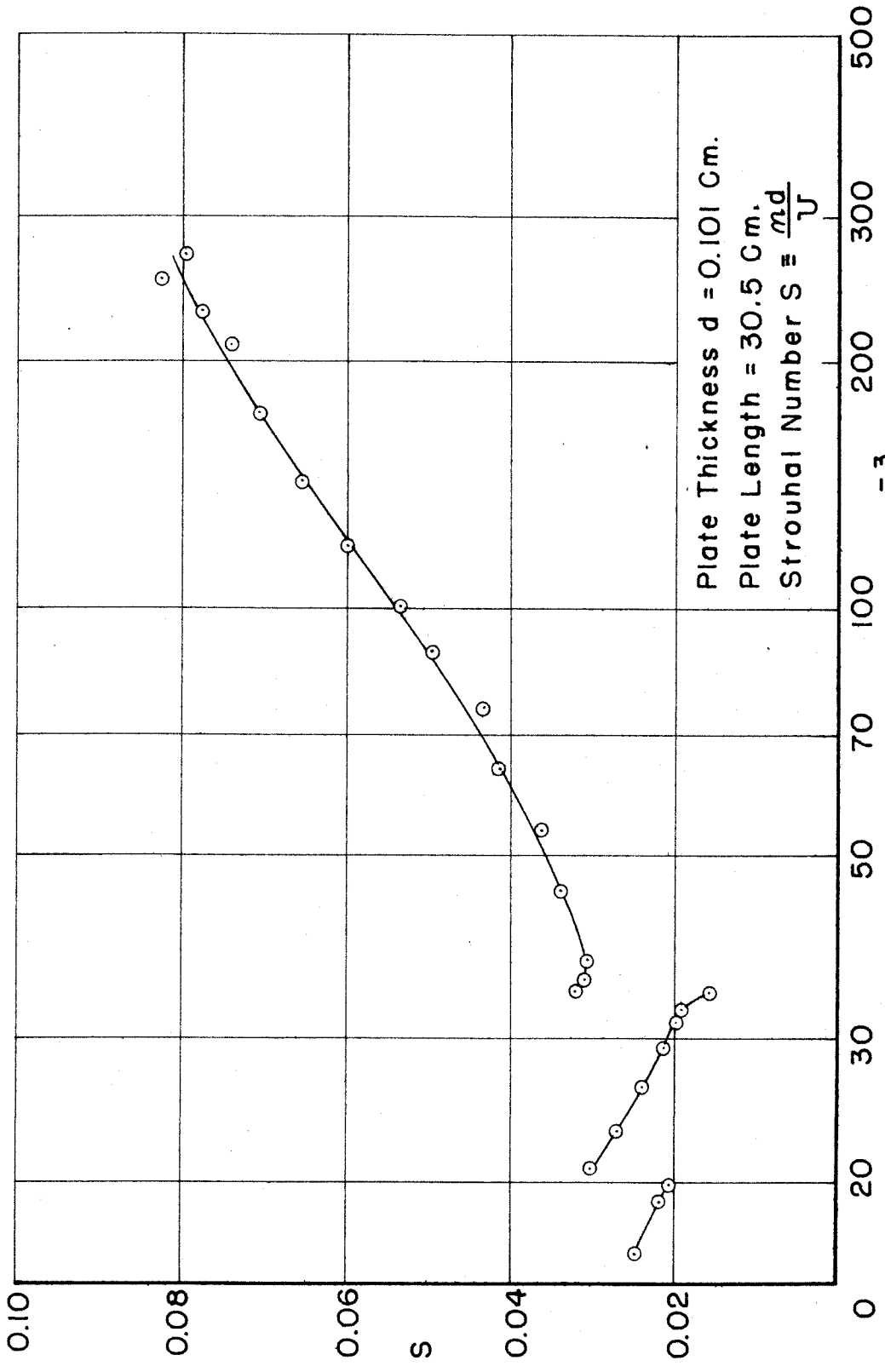

FIG. 6 - FLAT PLATE B - STROUHAL NUMBER VS. REYNOLDS NUMBER

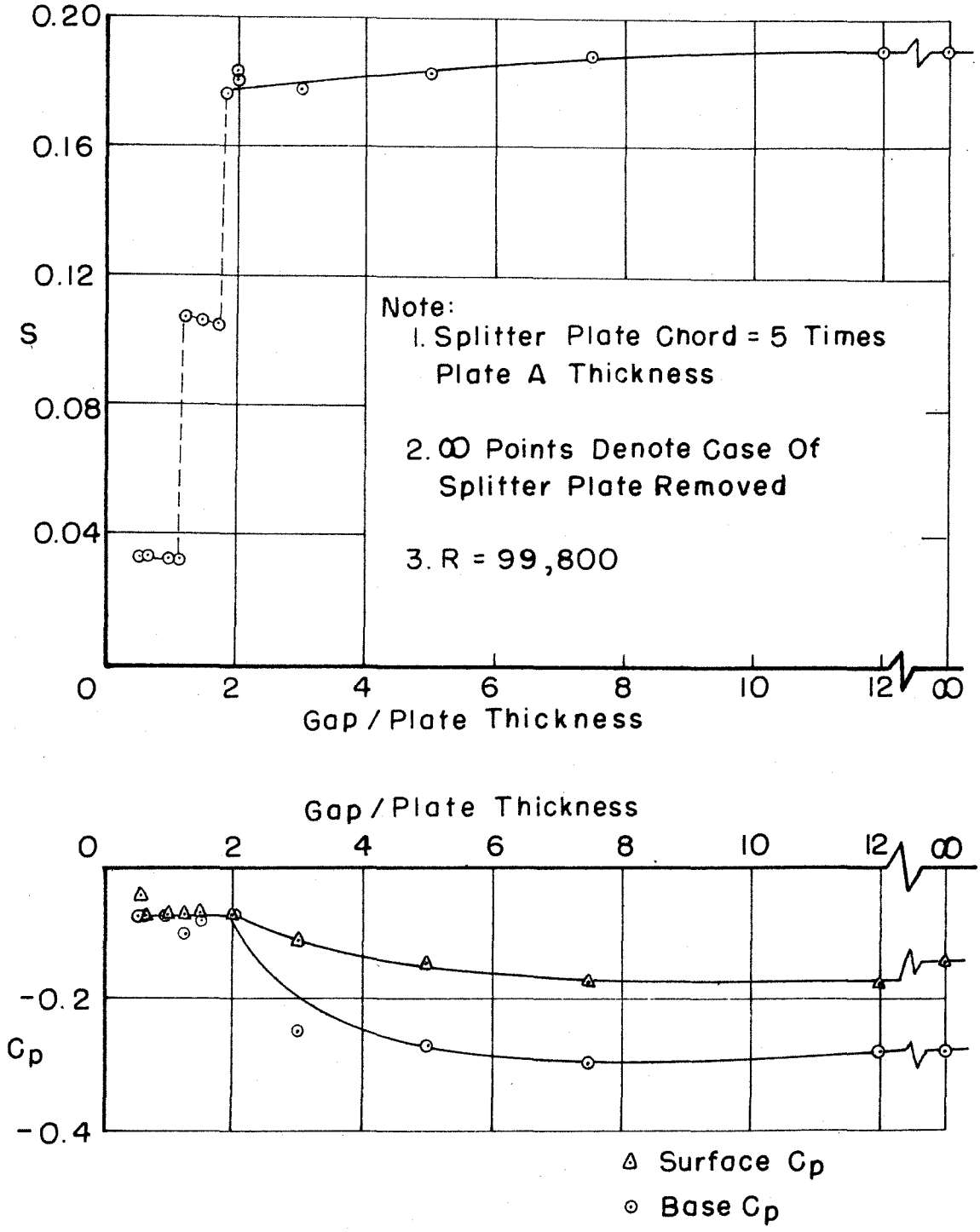

FIG. 7 – FLAT PLATE A WITH SPLITTER PLATE – EXPERIMENTAL STROUHAL NUMBER AND PRESSURE COEFFICIENTS VS. GAP DISTANCE BETWEEN PLATE A AND SPLITTER PLATE

Note: $\eta = \frac{y}{x}\sqrt{R}$

Where y = Height Above Plate Surface

x = Distance From Plate Leading Edge

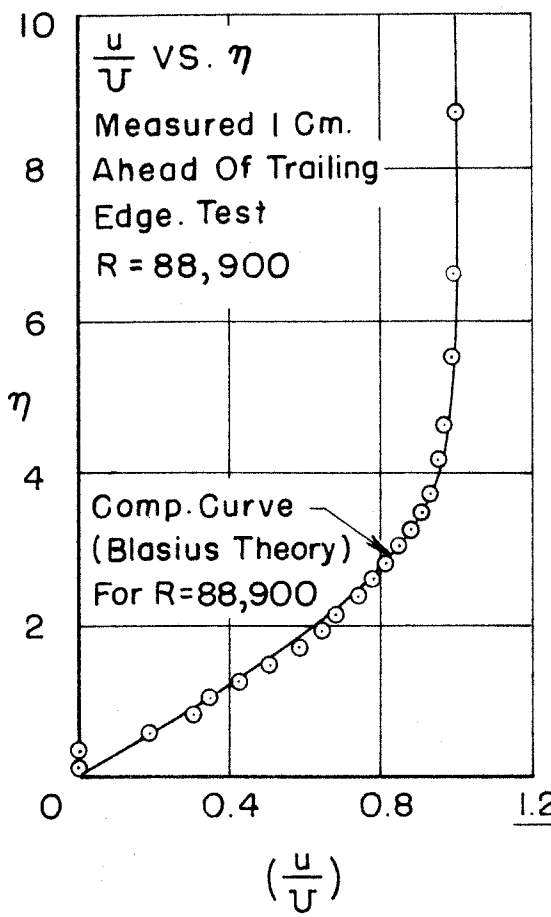

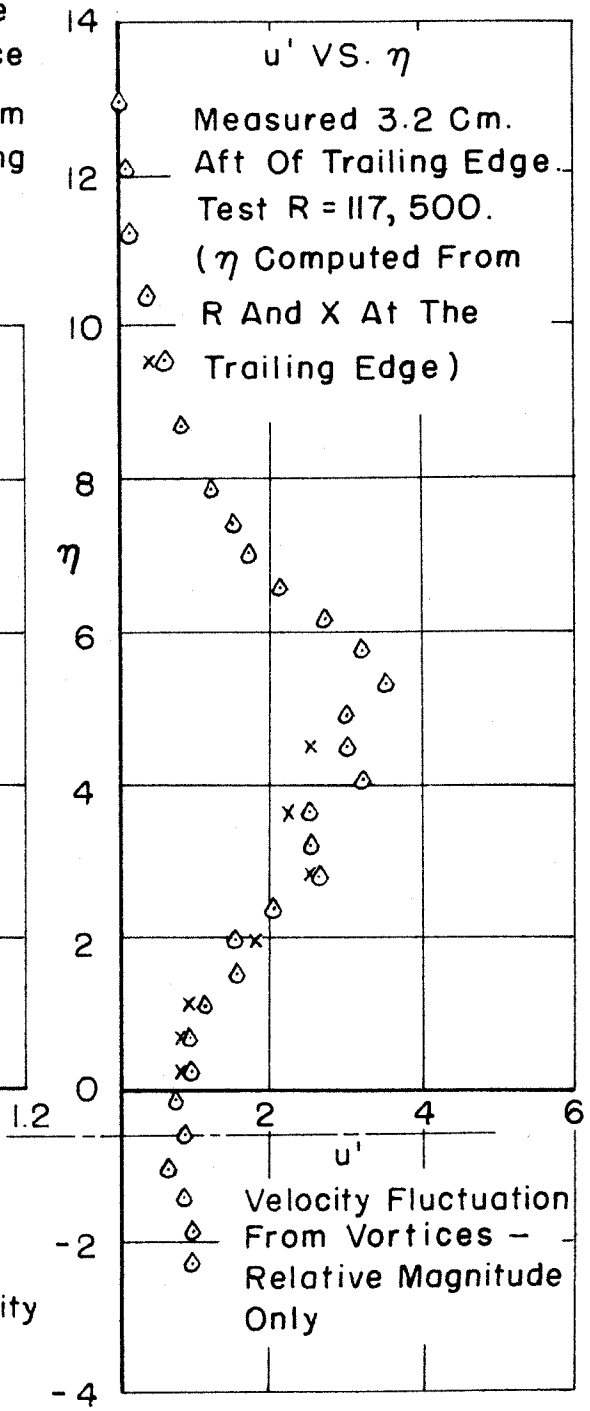

FIG. 8 – FLAT PLATE B – BOUNDARY LAYER AND VORTEX STREET MEASUREMENTS VS. NON-DIMENSIONAL HEIGHT ABOVE PLATE SURFACE

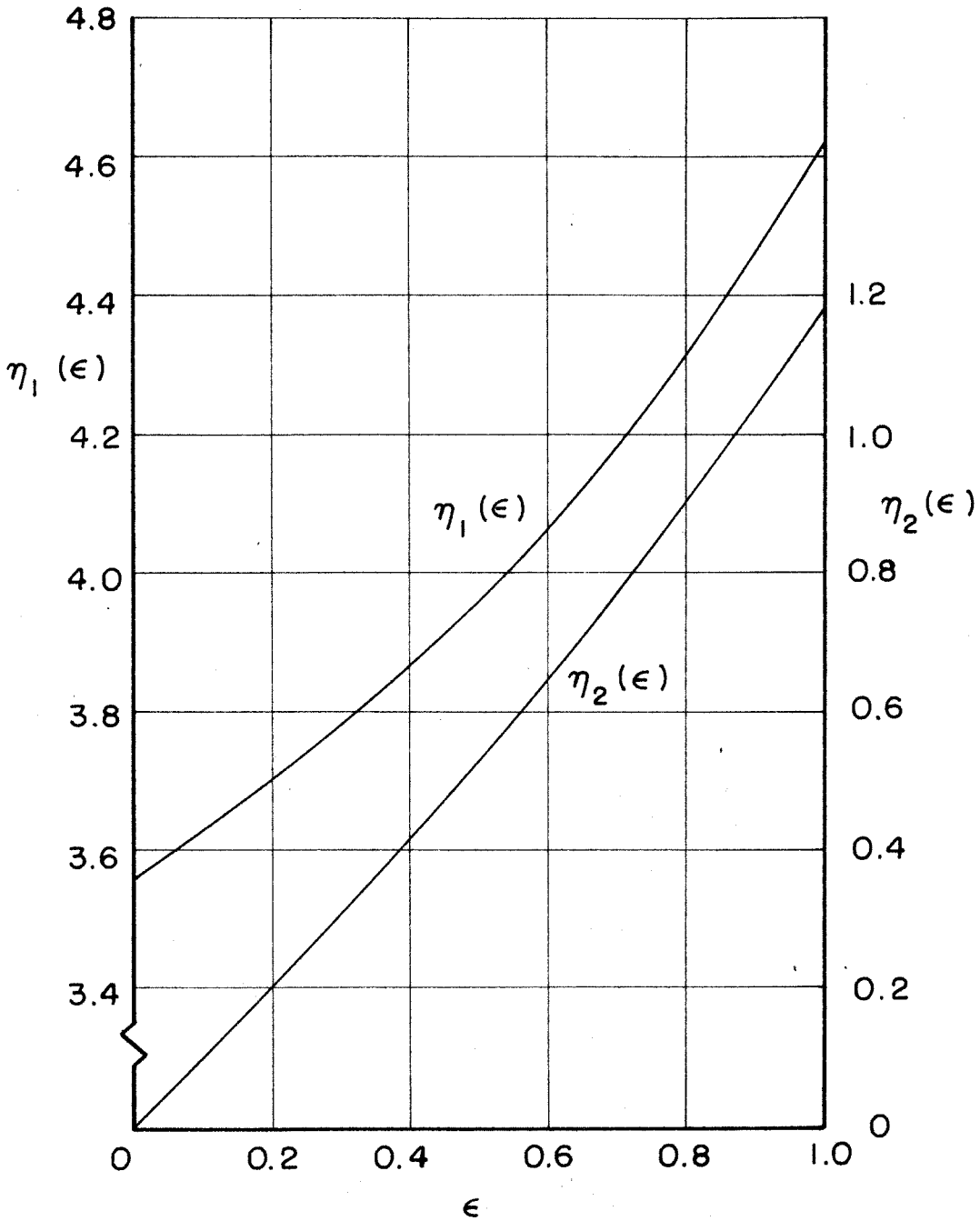

FIG. 9 — FUNCTIONS $\eta_1(\epsilon)$ AND $\eta_2(\epsilon)$

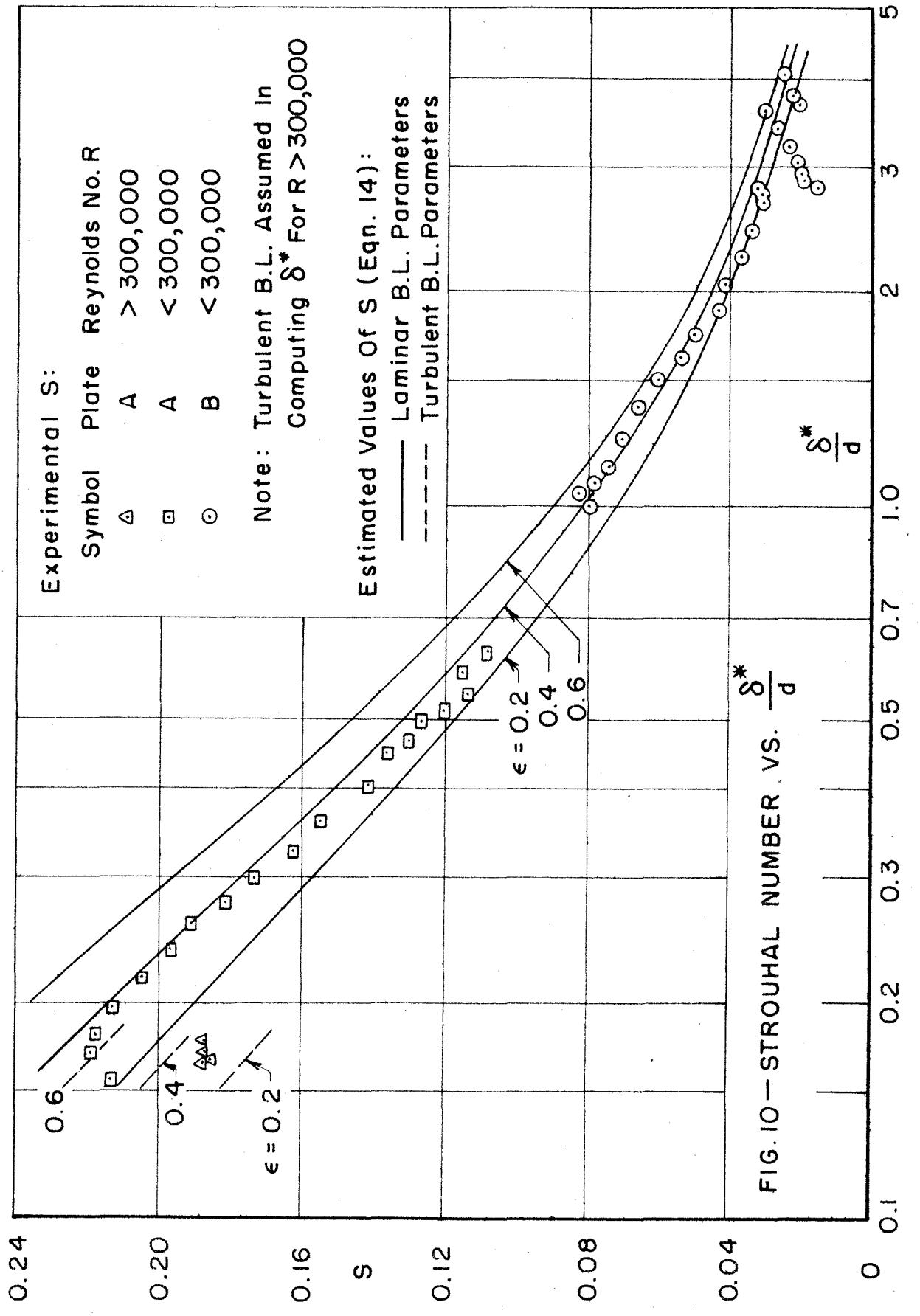

FIG. 10 — STROUHAL NUMBER VS. $\frac{\delta^*}{d}$

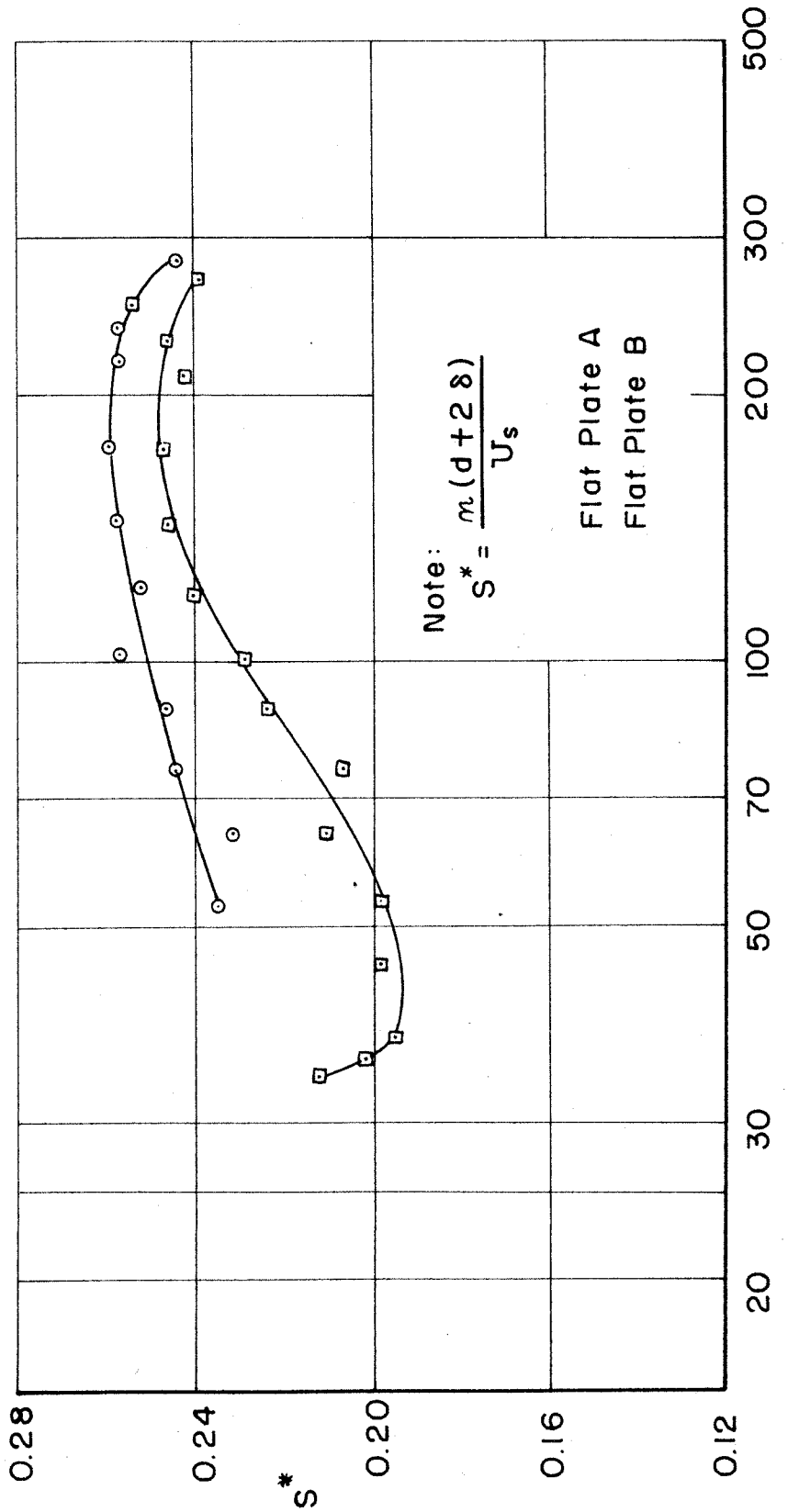

FIG. 11 – EXPERIMENTAL WAKE STROUHAL NUMBER VS. REYNOLDS NUMBER